Structural Biology and Molecular Biophysics

# Atomic-Level Free Energy Landscape Reveals Cooperative Symport Mechanism of Melibiose Transporter

Reviewed Preprint
v1 • November 28, 2024
Not revised

**Ruibin Liang** ✉, **Lan Guan** ✉

Department of Chemistry and Biochemistry, Texas Tech University, Lubbock, United States • Department of Cell Physiology and Molecular Biophysics, Center for Membrane Protein Research, Texas Tech University Health Sciences Center, School of Medicine, Lubbock, United States



**eLife Assessment**

In this potentially **important** study, the authors employed advanced computational techniques to explore a detailed atomistic description of the mechanism and energetics of substrate translocation in the MelB transporter. The overall approach is **solid** and reveals the coupling between sodium binding and melibiose transport through a series of conformational transitions, and the results for a mutant are also in qualitative agreement with the experiment, providing further support to the computational analyses. Nevertheless, the level of evidence is considered **incomplete** since there are concerns regarding the convergence and initial guess of the string calculations, leaving doubts that the computed pathway does not reflect the most energetically favorable mechanism.

https://doi.org/10.7554/eLife.103421.1.sa4

## Abstract

The Major Facilitator Superfamily (MFS) transporters are an essential class of secondary active transporters involved in various physiological and pathological processes. The melibiose permease (MelB), which catalyzes the stoichiometric symport of the disaccharide melibiose and monovalent cations (e.g., $Na^+$, $H^+$, or $Li^+$), is a key model for understanding the cation-coupled symport mechanisms. Extensive experimental data has established that positive cooperativity between the cargo melibiose and the coupling cation is central to the symport mechanism. However, the structural and energetic origins of this cooperativity remain unclear at the atomistic level for MelB and most other coupled transporters. Here, leveraging recently resolved structures in inward- and outward-facing conformations, we employed the string method and replica-exchange umbrella sampling simulation techniques to comprehensively map the all-atom free energy landscapes of the $Na^+$-coupled melibiose translocation across the MelB in *Salmonella enterica* serovar Typhimurium ($MelB_{St}$), in comparison with the facilitated melibiose transport in a uniporter mutant. The simulation results unravel asymmetrical free energy profiles of melibiose translocation, which is tightly coupled to protein conformational changes in both the N- and C-terminal domains. Notably, the cytoplasmic release of the melibiose induces the simultaneous opening of an inner gate,

resulting in a high-energy state of the system. Periplasmic sugar binding and cytoplasmic melibiose released are dynamically coupled with changes in the internal gating elements along the translocation pathway. The outward-facing sugar-bound state is thermodynamically most stable, while the occluded state is a transient state. The binding of $Na^+$ facilitates melibiose translocation by increasing the melibiose-binding affinity and decreasing the overall free energy barrier and change. The cooperative binding of the two substrates results from the allosteric coupling between their binding sites instead of direct electrostatic interaction. These findings add substantial new atomic-level details into how Na+ binding facilitates melibiose translocation and deepen the fundamental understanding of the molecular basis underlying the symport mechanism of cation-coupled transporters.

# Introduction

Major facilitator superfamily (MFS) membrane transporters (MFS) are ubiquitous across all kingdoms of life, accounting for more than 25% of all transmembrane proteins, and exhibit a wide range of functions and substrate specificities. They are critical in various physiological processes, including the uptake of nutrients and drugs, as well as the expulsion of xenobiotics[1]. Certain human homologs have become promising targets for drug development due to their vital roles in nutrient and drug transport[2]. For example, the MelB homolog MFSD2A is crucial for the uptake of the essential lipid lysophosphatidylcholine in the brain[3]. Melibiose permease of *Salmonella enterica* serovar Typhimurium ($MelB_{St}$) is a MFS sugar symporter that facilitates the simultaneous translocation of one galactoside-containing disaccharide (e.g., melibiose) and one cation (e.g., $Na^+$, $H^+$, or $Li^+$) across the membrane in the same direction, with a strict 1:1 stoichiometric ratio [4] (**Fig. 1**). This symporter is a well-established and useful model for studying the cation-coupled transport mechanisms of MFS transporters[1, 4–8]. It has been experimentally well-characterized by various biochemical/biophysical techniques in combination with genetic modification[9–15] and structural analysis[4, 16–19]. Additionally, extensive experimental data has been made available for MelB of *E. coli*[20–27]. Consistent results on the molecular recognitions for the galactoside and cation and their cooperative binding led to a hypothesis that the cooperative binding of melibiose and the coupling cation is critical for the symport mechanism[10, 28]. More recently, the correlations between substrate-binding affinities and protein conformational states have been identified through structural and binding analyses[19, 29]. While the cation-binding affinity appears largely independent of protein conformation, it was hypothesized that the sugar-binding affinity significantly decreases when $MelB_{St}$ is in the inward-facing (IF) state[19, 29].

To date, the structures for two major conformational states of $MelB_{St}$ have been resolved: the apo- or sugar-bound outward-facing (OF) state[16, 17], and the sugar-released, $Na^+$-bound IF state[18]. However, the molecular mechanisms underlying the coupled symport of the two substrates remain poorly understood. Crucial information regarding the structures, energetics and dynamics of the intermediate states (**Fig. 1**) during the transitions between the two major conformational states remains scarce. Furthermore, previous experiments have established that the binding of the two substrates is cooperative[28], but the structural and energetic basis of this cooperativity remains unclear. Although the regions of the mobile energy barriers for regulating the sugar translocation have been identified[19], the global free energy landscape of the entire sugar translocation process— encompassing sugar-binding and releasing events along with conformational transitions between the OF and IF conformations—remains largely unknown. The lack of quantitative characterization of such free energy landscapes has impeded a fundamental understanding of the complex interplays between the shifting of the mobile barriers and the cooperative binding of the two substrates.

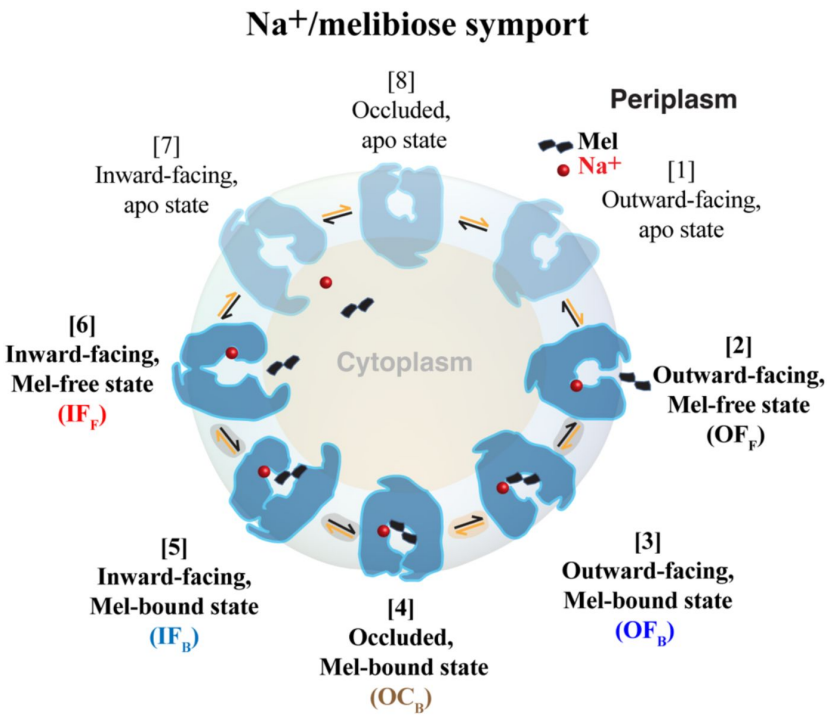


**Figure 1.**

The transport cycle of the MelB symporter. The current study describes the melibiose (Mel, black double square) translocation between the periplasm and cytoplasm in the presence or absence of a bound coupling cation ($Na^+$, red dot). The translocation of melibiose into cytoplasm starts from the $OF_F$ state ([2]) and proceeds to the $IF_F$ state ([6]) through several intermediate states such as the $OF_B$ ([3]), $OC_B$ ([4]), and $IF_B$ ([5]). Reversal of this process results in melibiose translocation into periplasm. These key intermediate states are highlighted in bold text, with the protein depicted in solid colors. See the main text for a detailed definition of the states.

Molecular simulations can fully elucidate the structures, dynamics, and thermodynamics of the transport cycle at atomic-level detail. However, calculating the sugar-translocation free energy landscape is a highly challenging task, because it requires sampling the large structural changes in the transporter coupled with substrate binding/unbinding processes. Although numerous computational studies have mapped the free energy landscapes of secondary active transporters and uniporters[30–42], none characterized the entire substrate translocation process coupled to global protein conformational transitions in cation-coupled MFS transporters. In addition, to the best of our knowledge, there has been no study on the structural and energetic origins of the cooperative transport of two substrates in cation-coupled MFS transporters.

To this end, we calculated the free energy profiles for the translocation of the melibiose across the WT $MelB_{St}$ in the $Na^+$-bound and -unbound states, as well as the uniport D59C mutant. Building upon the recently resolved structures for both OF and IF states[17, 19], the string method[43, 44] was employed to identify the minimum free energy pathway (MFEP) for the translocation of the melibiose molecule from the periplasmic to cytoplasmic sides, accompanied by the OF to IF conformational transition. Extensive replica-exchange umbrella sampling (REUS) simulations were performed along the MFEP to quantify the free energy surfaces of melibiose translocation with or without a bound $Na^+$. The simulations correspond to the experimentally observed melibiose exchange[4, 9, 16, 17, 45] driven by melibiose concentration gradients without cation transduction (**Fig. 1**). Explicit characterization of the thermodynamics underlying the entire melibiose translocation process reveals the structural and energetic underpinnings of how the sugar translocation across $MelB_{St}$ is facilitated by the binding of the coupling cation $Na^+$. To the best of our knowledge, this work is the first time that the free energy landscape dictating the functional cycle of a cation-coupled MFS symporter is characterized at full atomic-level detail, thus significantly deepening our understanding of cation-coupled transporters in general.

# Results

## Melibiose translocation coupled to protein conformational changes

The **Fig. 2** depicts the free-energy profile (or potential of mean force, (PMF)) for the melibiose translocation from the periplasmic to the cytoplasmic sides of the membrane through the WT $MelB_{St}$ with a $Na^+$ bound at the cation-binding pocket. The free energy changes ($\Delta G$'s) and barriers ($\Delta G^{\ddagger}$'s) of key steps during the translocation are summarized in **Table 1**. The translocation process starts with a melibiose molecule in the periplasmic bulk and a $MelB_{St}$ in its outward-facing sugar-free state ($OF_F$) (image ID 0). Binding of melibiose from the periplasmic side leads to the outward-facing sugar-bound state ($OF_B$) (image ID 13, Fig. S1), which exhibited a $\Delta G$ of −5.0 kcal/mol (**Table 1**, $\Delta G_{OF\ binding}$). This corresponds to a 5.0 kcal/mol melibiose binding affinity when the $Na^+$-bound protein is in the OF conformation. Notably, this state has the lowest free energy in the entire translocation process and thus is thermodynamically most stable. Then, the protein conformational changes took the system from the $OF_B$ to the inward-facing sugar-bound state ($IF_B$) (image ID 19), overcoming a barrier of ~6.8 kcal/mol (**Table 1**, $\Delta G^{\ddagger}_{OF\ to\ IF}$) required for passing through the occluded transition state ($OC_B$) during the conformational transition. The $OC_B$ state is a transient state, and the $IF_B$ state is higher in free energy than the $OF_B$ state by ~6.4 kcal/mol (**Fig. 2**, **Table 1**). Then, the melibiose was released to the cytoplasmic side of the bulk solution, reaching the inward-facing sugar-free state ($IF_B$, image ID 32), leaving behind a $Na^+$-bound, sugar-free $MelB_{St}$. This cytoplasmic melibiose release process only needs to overcome a small $\Delta G^{\ddagger}$of ~2.8 kcal/mol (**Table 1**, $\Delta G^{\ddagger}_{OF\ to\ IF}$) and has a small $\Delta G$ of ~2.3 kcal/mol, indicating a lower melibiose-binding affinity of the IF than the OF conformations (~5.0 kcal/mol). The entire transport process has a net $\Delta G$ of ~3.7 kcal/mol (**Table 1** and **Fig. 2**) and an overall $\Delta G^{\ddagger}$ of ~8.4 kcal/mol (**Table 1** and **Fig. 2**).

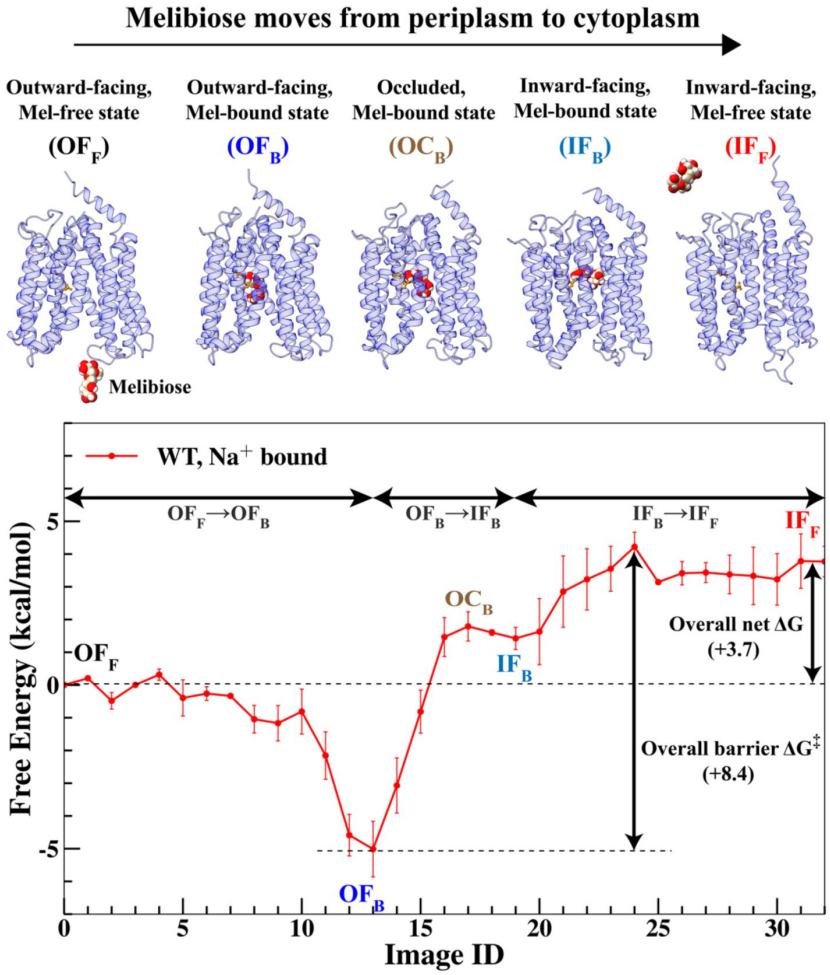


**Figure 2.**

The potential of mean force (PMF) for the translocation of the melibiose across the WT MelB$_{St}$ in the $Na^+$-bound state along the minimum free energy pathway (represented as a string of images 0 to 32). Top insets: representative snapshots of the MelB$_{St}$ (blue ribbons) and melibiose (spheres) in varied intermediate states. The bottom and top sides of each protein structure indicate the periplasmic and cytoplasmic sides of the membrane, respectively. The Asp19 and Asp124 residues, which are the major melibiose binding residues, are depicted as orange balls and sticks. The atoms in melibiose molecule are depicted as spheres.

| $\Delta G$'s and $\Delta G^{\ddagger}$'s | System | | |
|---|---|---|---|
| | WT, $Na^+$ bound | WT, $Na^+$ unbound | D59C, $Na^+$ unbound |
| Overall $\Delta G$ $(OF_F \rightarrow IF_F)$ | 3.7 | 11.8 | 8.3 |
| Overall $\Delta G^{\ddagger}$ $(OF_F \rightarrow IF_F)$ | 8.4 | 12.2 | 10.6 |
| $\Delta G_{OF\ binding}$ $(OF_F \rightarrow OF_B)$ | -5.0 | 1.4 | -2.0 |
| $\Delta G_{OF\ to\ IF}$ $(OF_B \rightarrow IF_B)$ | 6.4 | 7.0 | 5.3 |
| $\Delta G^{\ddagger}_{OF\ to\ IF}$ $(OF_B \rightarrow IF_B)$ | 6.8 | 8.0 | 5.3 |
| $\Delta G_{IF\ unbinding}$ $(IF_B \rightarrow IF_F)$ | 2.3 | 3.4 | 4.9 |
| $\Delta G^{\ddagger}_{IF\ unbinding}$ $(IF_B \rightarrow IF_F)$ | 2.8 | 3.8 | 5.3 |

**Table 1.**

**Free energy barriers (ΔG's) and net free energy changes ($\Delta G^{\ddagger}$'s).**

Free energy barriers and net free energy changes (in kcal/mol) for melibiose translocation in the WT $Na^+$ bound, WT $Na^+$ unbound, and the D59C mutant $Na^+$ unbound systems were analyzed for the overall translocation process and several key steps in this process.

To characterize the coupling between the melibiose translocations and protein conformational transitions, the free energy landscape was projected onto 2D free energy surfaces (FES) spanned by different combinations of collective variables (CVs) using Eq S4 (**Fig. 3**). In **Fig. 3A**, the 2D FES is spanned by the first principle component (PC1) of the backbone Cα atoms of all 12 transmembrane helices and the melibiose transport coordinate Z (see Method in SI for definition). As Z increases from −30 Å to +30 Å, the melibiose molecule moves through $MelB_{St}$ from the periplasmic to the cytoplasmic sides of the membrane. As the PC1 gradually increases from ∼-3.5 Å to +3 Å, the transmembrane helices transit from the OF to the IF conformational states.

As shown in **Fig. 3A**, the periplasmic sugar-binding process is correlated with dynamic fluctuations of the transmembrane helices, as exhibited by the shifts in the PC1 values across the multiple minima encountered in the $OF_F \rightarrow OF_B$ process. For example, from $OF_F$ (Z = −30 Å, PC1 = −3.2 Å) to $OF_B$ (Z = −3 Å, PC1 = −2.5 Å), the PC1 values fluctuate back and forth and has a net increase of ∼0.7 Å after reaching the $OF_B$ minimum. These fluctuations in PC1 correspond to non-negligible conformational fluctuations in the overall transmembrane protein backbones during the periplasmic-binding process. The binding-induced conformational change is more evident when the FES is projected to the 2D plane spanned by the translocation coordinate and the interhelical distance between helix I and VII near the periplasmic side of the membrane (**Fig. 3B**). There is a decrease in this interhelical distance from ∼22 Å at $OF_F$ to ∼19 Å at $OF_B$ as the melibiose approaches the binding site. Thus, the periplasmic sugar-binding slightly closes the periplasmic side of the sugar translocation pathway, preparing the protein for the subsequent conformational changes.

After the periplasmic sugar-binding event, the $OF_B \rightarrow IF_B$ process begins, largely increasing the PC1 from approximately −2.5 Å to +2 Å (**Fig. 3A**). This process features global protein conformational changes critical for the entire transport process. In this step, the sugar translocation pathway is fully closed on the periplasmic side and opened on the cytoplasmic side, preparing the protein for releasing sugar into the cytoplasm. A large decrease in multiple periplasmic interhelical distances is observed, such as between helices I and VII (from ∼19 Å to ∼14 Å) (**Fig. 3B**), as well as an increase in cytoplasmic interhelical distances, such as between the helices IV and X (from ∼13 Å to ∼20 Å) (**Fig. 3C**).

After the system reaches the $IF_B$ state, the melibiose release to the cytoplasmic bulk begins ($IF_B \longrightarrow IF_F$). The process goes through an intermediate state $IF_C$, where the melibiose passes through the most constricted region of the entire pathway contributed by Val145, Val346 (helix X), and Tyr369 (helix XI) (**Fig. 3A**). From $IF_B$ to $IF_C$, the cytoplasmic inter-helices distances further increase. For example, the distance between helices IV and X further increases to ∼23 Å near Z = + 11 Å to prepare the space for the melibiose to pass through (**Fig. 3A**). After this, the melibiose is eventually released to the cytoplasmic bulk and the interhelical distance between helices IV and X slightly decreases back to below 20 Å. The diagonal nature of the pathway linking $IF_B$, $IF_C$, and $IF_F$ (**Fig. 3C**) indicates that the motion of the substrate and the expansion/shrinkage of the cytoplasmic constricted region are tightly coupled. The finding is significant because it reveals that bound melibiose does not passively wait for the cytoplasmic path to widen, as previously speculated. Instead, it actively induces protein conformational changes to move out. This observation redefines the alternation-access model, demonstrating that both the periplasmic binding and cytoplasmic release of melibiose are tightly coupled with protein conformational changes.

## Changes in the pore radius profile during melibiose translocation

The coupling between the conformational change and the melibiose translocation is also evident through analyzing the radius profiles of the internal cavities that form the sugar translocation path in different intermediate states. For example, we first monitored the radius of the cavity near the periplasmic bulk (Z = −25 Å) during the entire sugar translocation process. This radius slightly decreases during periplasmic binding ($OF_F \rightarrow OF_B$, red vs. orange curves in **Fig. 4A**). It then

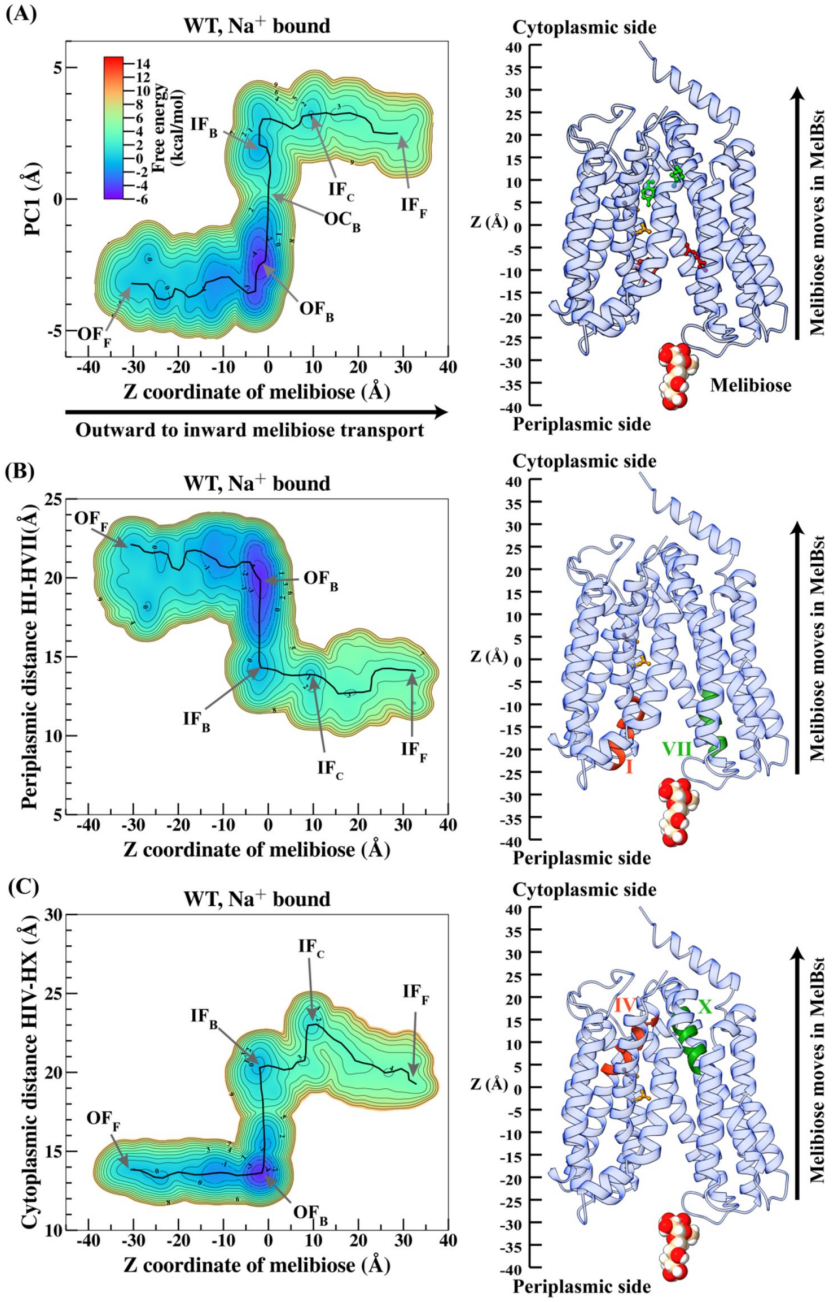


## Figure 3.

Free energy surfaces (FES) for the transport of the melibiose through the WT $MelB_{St}$ in the $Na^+$ bound state. (A) FES spanned by the first principle component of the backbone (PC1) vs. melibiose transport coordinate Z. An illustrative structure indicating the scale of the Z coordinate is shown on the right, and key residues in the periplasmic gate, binding site and cytoplasmic gate are highlighted in red, orange and green, respectively (see main text). (B) FES spanned by interhelical distance between helices I and VII on the periplasmic side. An illustrative structure indicating the helices I (red) and VII (green) is shown on the right. (C) FES spanned by interhelical distance between helices IV and X on the cytoplasmic side. An illustrative structure indicating the helices IV (red) and X (green) is shown on the right. The approximate minimum free energy pathways (MFEP) tracking the major basins on the FES are indicated as black lines, and the regions corresponding to the intermediate states are labeled by arrows. All FES plots share the same color bar as (A).

largely decreases by more than 3 Å during conformational transition ($OF_B \rightarrow IF_B$, orange vs. green curves in **Fig. 4A**). Following this, it remains almost the same during cytoplasmic release ($IF_B \rightarrow IF_F$, green vs. blue curves in **Fig. 4A**). Monitoring the radius of the cavity near the cytoplasmic bulk (Z = + 25 Å), it remains small below 2 Å during the periplasmic binding, and then increases by approximately 3 Å following the $OF_B \rightarrow IF_B$ transition. Thus, in general, the $OF_F \rightarrow IF_F$ process is accompanied by the widening and shrinking of the periplasmic and cytoplasmic terminals of the path in a reciprocal manner.

The radius profile also revealed two constricted regions surrounding the bound sugar molecular, which functions as gates on both the periplasmic and cytoplasmic sides of the sugar translocation path. The periplasmic constriction region is located near Z = −15 to −10 Å and formed by the cavity-lining residues, particularly the Tyr26 and Met27 on the kink of the helix I, and Asn248 and Asn251 on the helix VII (**Fig. 4A, right panel**). Clearly, the helix I kink moves towards the helix VII positioning in the middle of the melibiose-accessing path upon melibiose binding. Tyr26 frequently interacts with the melibiose as it passes through and defines the periplasmic edge of the sugar-binding pocket, and its extended bulky sidechain partially occludes the bound sugar from the periplasmic side. This constricted region is further narrowed when $MelB_{St}$ changes to the occluded transition state. Thus, the Tyr26 functions as a key gating residue. Experimentally, mutation of the Tyr26 to Cys26 residue resulted in the loss of active transport of the $MelB_{St}$, highlighting the importance of this residue in the functional cycle[13]. The cytoplasmic constriction region is located near Z = +11 Å, which is formed by the cavity-lining residues Val145, Val346 and Tyr369, as discussed above. When the periplasmic side of the transporter is open, the N- and C-terminal domains on the cytoplasmic side form a tightly connected salt-bridge network, as described previously[13, 17]. These ionic interactions majorly contribute to forming the inner barrier of cytoplasmic sugar release. As the melibiose passes through this region, the radius in this region expands to accommodate its motion (**Fig. 4C**), in line with the above-mentioned observation from the FES (**Fig. 3C**).

Another important observation is that periplasmic binding reduces the radius of the sugar-binding pocket (**Fig. 4B**), reaffirming the binding-induced conformational change discussed above (**Fig. 3**). The subsequent OF to IF conformational changes ($OF_B \rightarrow IF_B$) increase the radius of the sugar-binding cavity near Z = −2.5 Å (**Fig. 4B**). The expansion of the binding pocket eventually facilitates the release of melibiose to the cytoplasmic side. This is consistent with the results from the free energy profile calculation. The simulation results thus corroborate the previous experimental result[19] that the outward-facing conformation has a higher sugar-binding affinity than the inward-facing (**Fig. 2**-**3**) and explain its structural and energetic origin with atomic-level detail.

## Cooperative motion of N- and C-terminal domains

Multiple helices in both the N- and C-terminal domains change their relative orientation with respect to the normal of the membrane plane during the melibiose translocation. To quantify this observation, the free energy of the system is projected to 2D surfaces spanned by two collective variables (CVs), which measure the directional tilt angle of a helix with respect to the membrane plane normal (see “Method” for definition) and melibiose translocation. Based on the topographies of the 2D FES’s (Fig. S4 B-G), it is obvious that in the N-terminal domain, all helices decrease their tilting angles by 10-15 degrees as Z moves from −35 to 35 Å. In contrast, in the C-terminal domain, all helices increase their tilt angles by 10-20 degrees as Z moves from −35 to 35 Å (Fig. S4 H-M). The simultaneous tilting of all helices suggests that both domains must reorient with respect to the membrane normal to complete the global protein conformational transition. This transition exhibits a symmetric-like movement of the two pseudo-symmetric helix bundles. Notably, this finding, which cannot be derived from experimental structures alone due to the lack of a membrane surface, helps resolve a longstanding debate regarding the alternating-access model.

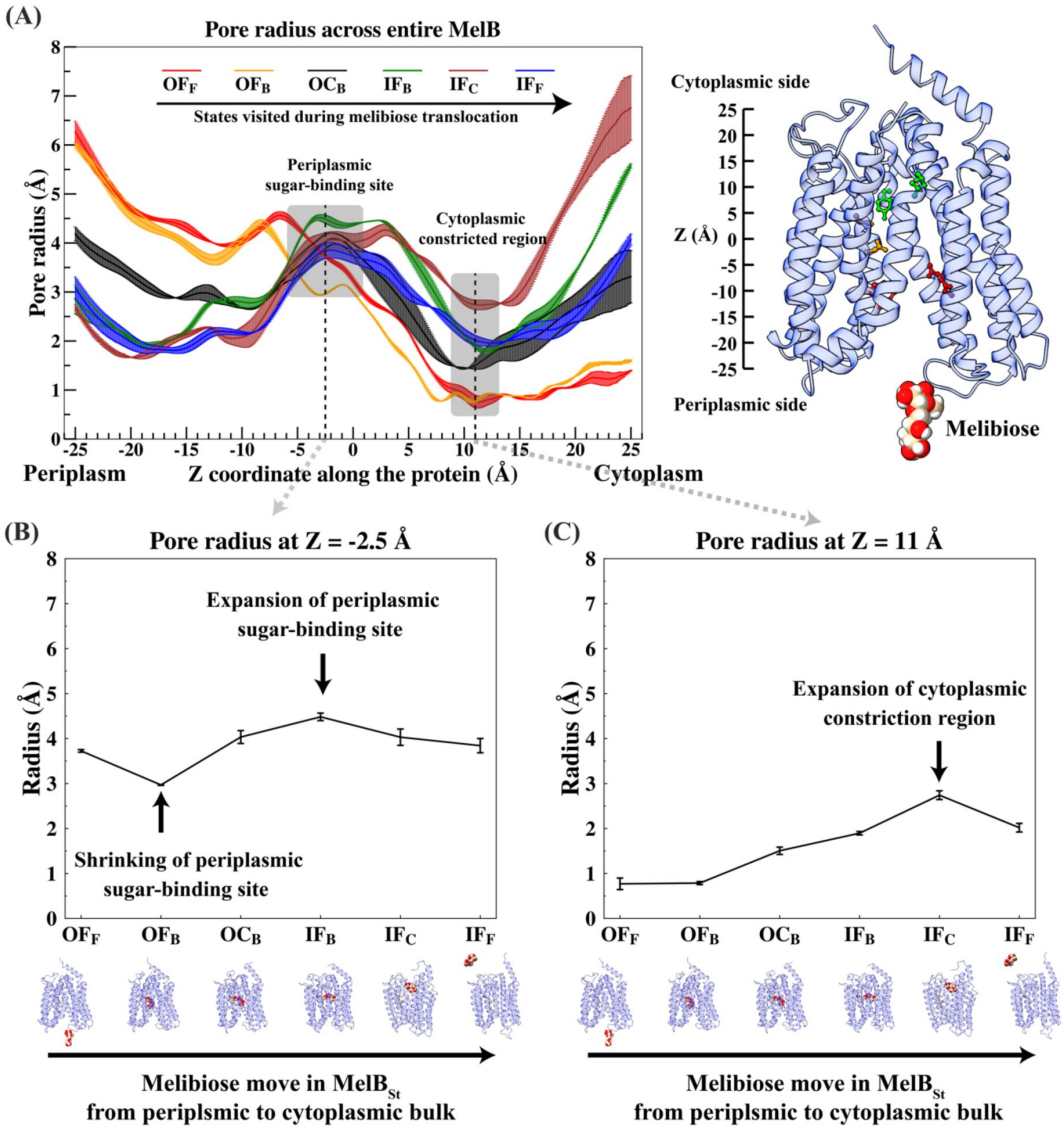


**Figure 4.**

Change of pore radius profile coupled to melibiose transport through WT $MelB_{St}$ in the $Na^+$ bound state. (A): Pore radii profile across the MelB as a function of the Z coordinate (relative to the COM of Asp124 and Asp19) along the entire protein (x-axis) for each different state during the melibiose translocation. As the melibiose is translocated from the periplasm to cytoplasm, the system transitions from the $OF_F$ (red) to $IF_F$ (blue) states through the $OF_B$ (orange), $OC_B$ (black), $IF_B$ (green), and $IF_C$ (brown) intermediate states, each of which features different pore radius profiles. The $IF_C$ state corresponds to the melibiose passing through the cytoplasmic constricted region near Z=11 Å. An illustrative structure indicating the scale of the Z coordinate is shown on the right. (B) and (C): Translocation of melibiose from the periplasmic to cytoplasmic sides of $MelB_{St}$ induces the change of pore radii measured at Z=-2.5 Å (periplasmic sugar-binding site) and Z=11 Å (cytoplasmic constricted region). The melibiose translocation process is represented as the transitioning of the system from the $OF_F$ to $IF_F$ states through multiple intermediate states along the x-axes. The protein structures below the plots serve as visual guides for the location of the melibiose in different states.

## Melibiose translocation energetically coupled to $Na^+$ binding

Next, we characterize the PMF of melibiose translocation when the $MelB_{St}$ is in the $Na^+$-unbound state (**Fig. 5**, blue curve; **Table 1**). The comparison between the PMFs of $Na^+$-unbound and the $Na^+$-bound states is essential for understanding how the $Na^+$ binding cooperates with the thermodynamics and kinetics of melibiose translocation. When the $Na^+$ is unbound, the overall net $\Delta G$ and overall barrier $\Delta G^{\ddagger}$are ~11.8 kcal/mol and ~12.2 kcal/mol, respectively (**Table 1**). These values are greater than the $Na^+$-bound state by 8.1 kcal/mol and 3.8 kcal/mol, respectively, indicating that the melibiose translocation is thermodynamically and kinetically less favorable if the $Na^+$ is unbound. Several factors contribute to the more endergonic and slower translocation process in the absence of bound $Na^+$. First, periplasmic melibiose binding (image IDs from 0 to 15) is endergonic with $\Delta G_{OF\ binding} \sim 1.4$ kcal/mol, in contrast to the exergonic process in the $Na^+$ bound state ($\Delta G_{OF\ binding} \sim -5.0$ kcal/mol). Second, the endergonic protein conformational transition (image IDs from 15 to 21) exhibits $\Delta G_{OF\ to\ IF} \sim 7.0$ kcal/mol and $\Delta G^{\ddagger}_{OF\ to\ IF} \sim 8.0$ kcal/mol, which are both greater than the $Na^+$ bound state (6.4 kcal/mol and 6.8 kcal/mol, respectively). Third, the endergonic cytoplasmic unbinding event (images 21 to 32) exhibits $\Delta G_{IF\ binding} \sim 3.4$ kcal/mol and $\Delta G^{\ddagger}_{IF\ unbinding} \sim 3.8$ kcal/mol, again greater than the $Na^+$ bound state (2.3 kcal/mol and 2.8 kcal/mol, respectively).

The well-characterized D59C mutation results in a melibiose uniporter due to the loss of the carboxyl group on the Asp59, which is the only residue critical for binding of all three types of coupled cations ($Na^+$, $H^+$, and $Li^+$)[12, 18, 28]. This mutant thus loses cation-coupled active transport activity but can facilitate the transport of melibiose downhill its concentration gradient[17] and the exchange of melibiose across the membrane [16]. This unique feature makes the mutant a good model system for understanding the $Na^+$/melibiose symport mechanism.

The melibiose translocation across the D59C mutant has an overall net $\Delta G$ of ~ 8.3 kcal/mol and overall free energy barrier $\Delta G^{\ddagger}$ of 10.6 kcal/mol (**Fig. 5**, green curve; **Table 1**). They are both greater than the WT $Na^+$ bound system (3.7 kcal/mol and 8.4 kcal/mol, respectively), making the melibiose translocation thermodynamically and kinetically less favorable. Several factors contribute to the more endergonic and slower melibiose translocation in the mutant. The periplasmic sugar binding (image IDs from 0 to 13) has a $\Delta G_{OF\ binding}$ of ~ −2.0 kcal/mol, indicating that the mutation diminishes the binding affinity of the OF state by ~3.0 kcal/mol as compared to the WT $Na^+$-bound system. Unlike the WT $Na^+$-unbound system, the periplasmic binding in the D59C mutant is exergonic despite its incapability of binding cations, which is consistent with previous experiential measurements[17]. After the $OF_B$ state is reached, the $OF_B \longrightarrow IF_B$ transition together with the cytoplasmic sugar release ($IF_B \longrightarrow IF_F$) (image IDs from 13 to 32) results in a combined high barrier of ~10.6 kcal/mol ($\Delta G_{OF\ to\ IF} + \Delta G^{\ddagger}_{IF\ unbinding}$). This rate-limiting barrier in the mutant is ~2.2 kcal/mol higher than the WT $Na^+$ bound system. Notably, the mutant features ~3 kcal/mol higher barrier for the cytoplasmic sugar release, which is likely caused by the different orientations of the residues lining the cytoplasmic constricted region.

In both $Na^+$ unbound systems (WT and D59C), as expected, melibiose translocation is still coupled with protein conformational changes, but to a lesser extent than in the WT, $Na^+$ bound system (Figs. S5-S10). In both $Na^+$ unbound systems, periplasmic binding and cytoplasmic release are coupled with changes in the overall conformation of the protein and specific interhelical distances (Figs. S5-S6), as well as pore radius of the sugar-binding pocket and cytoplasmic constricted region (Figs. S7-S8). These changes are smaller in scale compared to the WT though. The directional tilt angles of helices in the N- and C-terminal domains follow the same trend as the WT $Na^+$ bound system (Figs. S9-S10).

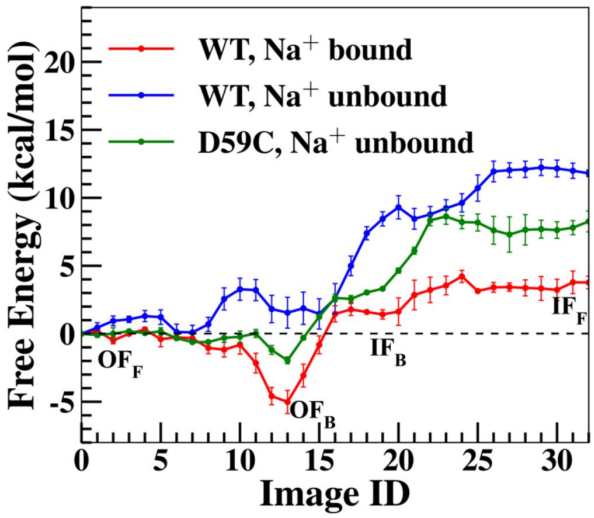


**Figure 5.**

PMFs for the transport of the melibiose across $MelB_{St}$ along the MFEPs represented as strings of images (0 to 33). The PMFs are calculated in the WT, $Na^+$ bound (red) and unbound (blue) states, and the D59C mutant in the $Na^+$ unbound state (green).

Overall, the removal of $Na^+$ from the cation-binding site, either due to low $Na^+$ concentrations in bulk or loss of $Na^+$ binding site, can largely reduce melibiose binding affinity, as has been well-documented by a variety of experimental tests in varied methods[9, 12, 16–18, 28]. This is one of the key factors contributing to the increased overall $\Delta G$'s and $\Delta G^{\ddagger}$'s for the melibiose translocation in the two $Na^+$ unbound systems. These results explicitly demonstrate that the free energy profiles explicitly demonstrate that the co-transport of $Na^+$ and melibiose is a direct result of binding cooperativity between the two substrates.

## Allosteric coupling between $Na^+$ and melibiose binding

To understand the different melibiose binding affinities in the WT $Na^+$ bound and unbound systems, we performed a total of 500 ns unbiased MD simulations in the $OF_B$ state for each system. The interaction energies between the melibiose and $MelB_{St}$ are compared between these two systems (Fig. S11). The interaction energy is decomposed into contributions from electrostatic and van der Waals components (Fig. S11 A&B, green and red bars, respectively). Importantly, the direct interaction energy between the bound $Na^+$ and melibiose in the WT $Na^+$ bound system was also evaluated.

Upon the unbinding of $Na^+$ (Fig. S11A), the protein-melibiose interaction energy shifted from −113 ± 2 to −105.4 ± 0.5 kcal/mol in WT $MelB_{St}$, consistent with the reduction in the binding affinity of the melibiose. Such a reduction largely arises from the electrostatic component, which changes from −96 ± 2 to −88.0 ± 0.4 kcal/mol. Notably, the direct interaction energy between the bound $Na^+$ and melibiose (∼ 0.2 ± 0.5 kcal/mol) in the WT $Na^+$ bound state is negligible. This finding is important in that the decrease in the melibiose binding affinity upon $Na^+$ unbinding is not due to losing the direct $Na^+$-melibiose interaction but due to a weakened protein-melibiose interaction. The decreased melibiose-binding affinity in the absence of $Na^+$ is mainly attributed to the alteration of local electrostatic interactions between melibiose and its nearby residues (Fig. S11B).

The WT $Na^+$ bound system features a narrower distribution of the local melibiose-protein interaction energy that peaked at a lower energy range than the WT $Na^+$ unbound system (Fig. S12A). This implies that the $Na^+$ unbinding alters the binding cavity and disfavors melibiose binding. To further probe the structural origin of this effect, we analyzed the hydrogen-bonding interactions between the melibiose and protein (Table S1). $Na^+$ unbinding from the WT $MelB_{St}$ led to the loss of 0.9 ± 0.2 hydrogen bonds between the melibiose and protein. In addition, the hydrogen bonds with three charged residues Asp124, Asp19, and Arg149, which contribute most to the protein-melibiose hydrogen bonds in the $OF_B$ state, are affected by the $Na^+$ unbinding the most. Thus, the reduction of hydrogen bonds between melibiose with the protein contributes to decreased binding affinity in the absence of a bound $Na^+$ ion.

The change in the hydrogen-bonding interaction due to $Na^+$ unbinding likely results from the allosteric coupling between the cation-binding and melibiose-binding sites. The Asp124 and Tyr120 residues in helix IV are essential in the coupling pathway since this helix also contributes the Thr121 residue to the $Na^+$-binding site. Without a bound $Na^+$ ion, the distance between the Asp55 and Asp124 is elongated (Fig. S12B). The same trend is also observed for the distances between Asp124 and Asp19 (Fig. S12C), between Tyr120 and Asp55 (Fig. S12D), and between Tyr120 and Asp19 (Fig. S12E). Furthermore, the distance between Asp55 and Asp19, i.e., the two key residues in the cation- and sugar-binding sites, respectively, is increased upon $Na^+$ unbinding (Fig. S12F). The correlations between the changes in these pairwise distances suggest that both Asp124 and Tyr120 residues propagate structural changes from the $Na^+$-binding site to the sugar-binding site upon $Na^+$ unbinding, leading to a decrease in melibiose affinity. The unbinding of $Na^+$ weakens the hydrogen bond between Asp19 and the 3-hydroxyl group of melibiose, as indicated by their elongated separation distance (Fig. S12G). This observation aligns with previous

experimental studies[13, 16, 24, 27, 46]: the D124C or Y120C mutants can bind melibiose but lose $Na^+$-coupled melibiose active transport[16]. Our simulations thus provide an atomistic-level explanation for these experimental observations in these decoupling mutants.

## Discussion

Calculating the free energy landscape that describes the protein conformational transitions associated with substrate translocation through transporters is a challenging yet essential task for understanding their functional mechanisms. In this study, building upon two resolved ligand-bound structures representing the inward-[19] and outward-facing conformational states[17, 18], we uncovered a wealth of new mechanistic information about the functional cycle of MelB. This was achieved through extensive free energy calculations combined with state-of-the-art reaction path-finding techniques. Notably, the use of two experimental structures as initial guesses for the two endpoints of the minimum free energy pathway (outward-facing sugar-free and inward-facing sugar-free states) enhances the reliability of the string method (Fig. S3). This is an improvement over previous applications of this approach to other transporters, where only one major conformational state (outward-facing, inward-facing, or occluded) was experimentally available, and the other major conformations had to be generated by biased molecular dynamics simulations[31, 33, 35]. Our simulation results are consistent with a large body of experimental data collected in the past decades via varied biochemical and biophysical data and structural analyses[9, 10, 12, 13, 18, 19, 28].

First, all simulation data consistently showed that $Na^+$ binding increases the melibiose-binding affinity of WT $MelB_{St}$, in agreement with previous experimental measurements[9, 28]. Second, the free-energy landscape indicates that the inward-facing states are thermodynamically less stable than the outward-facing states, regardless of the binding of $Na^+$ and melibiose, providing the energetic data supporting the conclusion drawn from structural analysis[19]. Third, the overall free energy landscape reveals that the outward-facing conformation of the WT has the highest sugar-binding affinity, and the $OF_B$ state is the thermodynamically most stable state for the entire translocation process (**Table 1** & **Fig. 2**). This is a piece of direct evidence supporting that the IF conformational state has a lower sugar-binding affinity and the experimentally measured binding affinity is primarily related to the OF conformational state[19].

During the melibiose translocation, only a modest rate-limiting barrier is encountered in the $OF_B \rightarrow OF_F$ process (~5 kcal/mol, **Fig. 2**). The protein conformational transition and cytoplasmic release is a cooperative process that increases the free energy of the system. The opening of the cytoplasmic gate is narrow and is induced by the motion of the sugar, so the cytoplasmic sugar-release process can be appropriately described as sugar squeezing through the inner barrier. In addition, the lack of a thermodynamically stable occluded state ($OC_B$) facilitates the $OF_B \rightarrow IF_B$ transition. All these features make $MelB_{St}$ a highly effective transporter.

The free energy landscapes reveal the coupling mechanisms between the two substrates and the transporter, providing new insights into experimental measurements of $MelB_{St}$ and its mutants[10, 17, 19, 28]. Without $Na^+$, both WT and D59C mutants exhibit higher $\Delta G^{\ddagger}$and $\Delta G$ than the WT $Na^+$-bound system, making melibiose translocation less favorable. This suggests that the coupling between sugar and cation is primarily due to energetic coupling at the binding step. $Na^+$binding increases melibiose affinity, lowers the free energy barrier and change, and facilitates the protein conformational transition, thus accelerating melibiose translocation. The molecular basis underlying the difference in the free energy landscapes involves strengthened hydrogen bonds between melibiose and its binding residues (Asp19, Asp124, Arg149) due to $Na^+$ binding at the cation-binding pocket (Asp55, Asp59, Thr121, Asn58), with allosteric coupling through Asp124

and Tyr120 on helix IV, as proposed sed on experimental data[16, 24, 27, 46]. The interaction between the two binding sites underpins the energetic and kinetic coupling necessary for the cooperative transport of $Na^+$ and melibiose.

The WT $MelB_{St}$ mediates both the active transport and facilitated diffusion of melibiose [4]. In contrast, the D59C mutation eliminates the active transport mode of WT but retains its melibiose uniport activity[16, 17], similar to the E325A mutant of LacY[7, 47]. Although such a phenomenon is observed in the D59C MelB and has been an important clue for identifying the cation-binding site of cation-coupled secondary transporters (7, 47, 48), the molecular origin of why the mutant retains uniport activity remains elusive to date. Here, the comparison between the free energy landscapes of the WT and mutant offers a microscopic-level explanation. For the D59C mutant, the overall $\Delta G^{\ddagger}$ of melibiose translocation is modestly higher than WT, Na+ bound $MelB_{St}$ by only 2.2 kcal/mol (**Table 1**). Thus, this mutation does not kinetically block the inward sugar translocation entirely, and it can even facilitate the outward translocation process by reducing the periplasmic sugar-releasing barrier as a result of reduced binding affinity in the OF state (**Fig. 5**). Therefore, the bi-directional exchange and gradient-downhill transport of melibiose can still be observed so long as the melibiose concentration is high enough on at least one side of the membrane. Notably, the coupling between the melibiose translocation and conformational change in this uniporter mutant remains (Figs. S6, S8 & S10). From an evolutional point of view, it is likely that the introduction of a cation site into a uniporter can accelerate the substrate translocation and increase the substrate-binding affinity. This symport function evolved from a uniporter can better serve cellular needs by harvesting substrate from scarce conditions.

In summary, our all-atom free energy landscapes of $MelB_{St}$ provided numerous critical, novel and fundamental insights into the structural and energetic origins of the coupling mechanism essential in cation-coupled MFS symporters: (1) the substrate translocation is tightly coupled to global protein conformational changes where all transmembrane helices are reoriented with respect to the membrane normal, (2) periplasmic binding is coupled with a partial closure of the periplasmic gate and shrinkage of sugar-binding site, (3) the outward-facing sugar-bound state is thermodynamically most stable during the entire translocation process, (4) the occluded state is a transient state, (5) the melibiose cytoplasmic release is coupled to the temporary expansion of the cytoplasmic gate, and (6) the allosteric coupling between the cation- and sugar-binding sites leads to cooperative binding of $Na^+$ and melibiose, which facilitates sugar translocation thermodynamically and kinetically. For the first time, our free energy profiles explicitly demonstrate that the co-transport of $Na^+$ and melibiose is a direct result of binding cooperativity between the two substrates. Notably, although such cooperativity has been observed experimentally on a macroscopic level, our free-energy simulations comprehensively characterized this core mechanism of symport with atomic-level detail, and provide explicit, crucial evidence for energetic coupling between the two co-transported solutes across all intermediate states visited during the entire melibiose translocation process (**Figs. 1**-**2** & **5**).

# Methods

A brief summary of the methods is provided here, with full details included in the SI.

## System setup

Three simulation systems were prepared to calculate the free energy landscapes of melibiose translocation coupled with protein conformational transition: (1) WT $MelB_{St}$ with $Na^+$ bound, (2) WT $MelB_{St}$ without $Na^+$, and (3) D59C mutant without $Na^+$. The OF and IF conformational states were derived from crystal (PDB code 7L16[17]) and CryoEM (PDB code 8T60[19]) structures, respectively. Key steps in the structural preparation included mutating residues to match the

desired states, positioning melibiose in the binding site, adding a lipid bilayer, and neutralizing with 0.15M NaCl. Each system consisted of ~130,000 atoms in a simulation box of ~100 ×100 ×130 Å³. All systems were constructed using the CharmmGUI web interface[48].

## Preparation for string method simulations

Initial string images for string method simulations were prepared for all three systems. First, for melibiose binding/unbinding processes in OF and IF states, the system was relaxed with geometry optimization and then equilibrated with backbone restraints. The bound melibiose was gradually pulled out of the protein (cytoplasmic unbinding for the IF state and periplasmic unbinding for the OF state) using a series of harmonic potentials, creating intermediate snapshots for substrate release into both sides of the membrane. This provided initial string images for $OF_F \rightarrow OF_B$ and $IF_B \rightarrow IF_F$ transitions. Next, the geodesic interpolation algorithm[49] generated 10 intermediate images of the transmembrane backbone for the $OF_B \rightarrow IF_B$ conformational transition. These backbone structures guided restrained simulations that dynamically relaxed all atoms in the images. All simulations used the CHARMM36m[50–56] and TIP3P force fields[57], and were performed using the NAMD software package [58].

## String method simulations

The String Method with Swarms of Trajectories (SMwST)[43, 44] was employed to identify the minimum free energy pathway (MFEP) for melibiose translocation in all three systems. This method has been successfully applied to other types of secondary active transporters[31, 33, 35] and protein complexes[59]. The initial string consisted of 33 images, representing the entire $OF_F \leftrightarrow IF_F$ transition. These images were projected into a 13-dimensional space defined by CVs related to melibiose translocation and protein conformational changes.

The SMwST simulations involved 500 iterations, where each image was equilibrated and propagated in each iteration. The string was updated iteratively until convergence was achieved, as monitored by RMSD in the 13-D space (Fig. S2). The endpoints of the final string corresponded closely to the experimental OF and IF structures (Fig. S3).

## Replica-exchange umbrella sampling (REUS) simulations

The last iteration of the string from the SMwST simulation was used as the MFEP for performing REUS simulations[60, 61]. The 33 image centers were interpolated into equidistant 13-D window centers for 33 umbrella windows. A harmonic potential (0.5-1 kcal/mol) acted on each of the 13 CVs per window. Initial conditions for each window were taken from the images in the last SMwST iteration. Replica exchanges among 10 neighboring windows were attempted every 10 ps on a rotation basis[59]. The REUS simulations ran for 90 ns per window, with the first 10 ns discarded as equilibration, resulting in 7.9 μs of total sampling time for all three systems.

## Analysis

The REUS simulations were unbiased using a generalized version[33] of the weighted histogram analysis method[62, 63] (Eqs. S1-S2). The free energies of each image were corrected using Eq S3. The 2D free energy surfaces were constructed using Eq. S4. The MFEP connecting the $OF_F$ and $IF_F$ states on the 2D free energy surfaces (FES) was traced using the zero-temperature string method. The HOLE program[64] was used to analyze the pore radius profiles for all snapshots sampled by the REUS simulations.

# Data Availability Statement

The data supporting this article have been included in the Supplementary Information.

## Acknowledgements

This work was supported by the National Institutes of Health Grants R35GM150780 to R.L. and R35GM153222 to L.G. The researchers used GPU computing facilities provided by the High-Performance Computing Center at Texas Tech University. The authors also acknowledge the helpful insights and inputs provided by Prof. Abhishek Singharoy at Arizona State University, and the initial simulation system setup by Mr. Amirhossein Bakhtiiari at Texas Tech University.

## Additional information

### Author contributions

The manuscript was written through the contributions of all authors. Ruibin Liang designed the research, performed the simulations, analyzed the data, and wrote the manuscript. Lan Guan designed the research and revised the manuscript. All authors have given approval to the final version of the manuscript.

### Conflict of interest

The authors declare no competing financial interests.

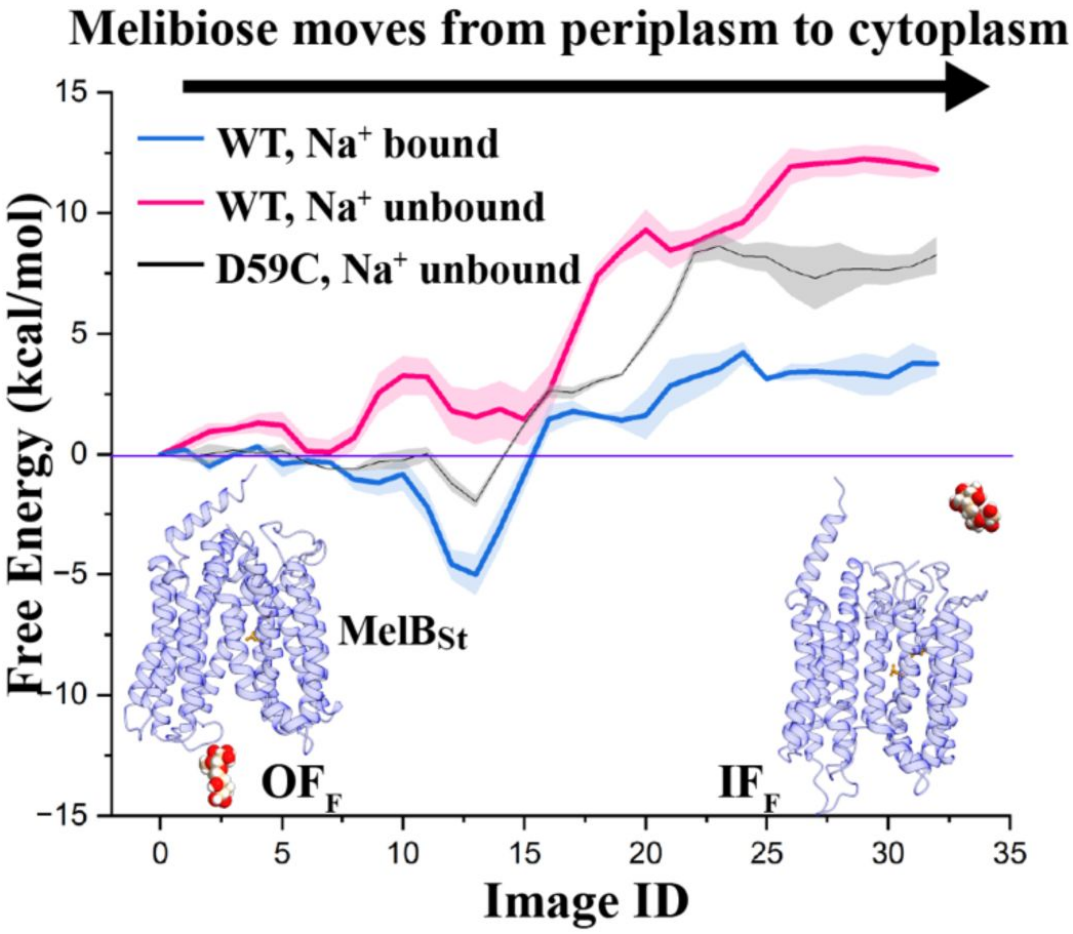

All-atom free energy landscapes of the entire melibiose translocation process in wild-type $MelB_{St}$ and its uniport D59C mutant elucidate the structural and energetic basis of the positive cooperativity between melibiose and its driving cation. The new insights significantly deepen our understanding of the molecular basis underlying cation-coupled transport mechanisms in MFS symporters.

# References


1. Saier M. H. *et al.* (1999) **The major facilitator superfamily** *J Mol Microbiol Biotechnol* **1**:257–279

2. Lin L., Yee S. W., Kim R. B., Giacomini K. M. (2015) **SLC transporters as therapeutic targets: emerging opportunities** *Nat Rev Drug Discov* **14**:543–560

3. Nguyen L. N., Ma D., Shui G., Wong P., Cazenave-Gassiot A., Zhang X., Wenk M. R., Goh E. L., Silver D. L. (2014) **Mfsd2a is a transporter for the essential omega-3 fatty acid docosahexaenoic acid** *Nature* **509**:503–506

4. Guan L. (2018) **Na(+)/Melibiose Membrane Transport Protein** *MelB.Journal* https://doi.org/10.1007/978-3-642-35943-9_10082-1

5. Niiya S., Moriyama Y., Futai M., Tsuchiya T. (1980) **Cation coupling to melibiose transport in Salmonella typhimurium** *J. Bacteriol* **144**:192–199

6. Poolman B., Knol J., van der Does C., Henderson P. J., Liang W. J., Leblanc G., Pourcher T., Mus-Veteau I. (1996) **Cation and sugar selectivity determinants in a novel family of transport proteins** *Mol. Microbiol* **19**:911–922

7. Guan L., Kaback H. R. (2006) **Lessons from lactose permease** *Annu. Rev. Biophys. Biomol. Struct* **35**:67–91

8. Yan N. (2015) **Structural Biology of the Major Facilitator Superfamily Transporters** *Annu Rev Biophys* **44**:257–283

9. Guan L., Nurva S., Ankeshwarapu S. P. (2011) **Mechanism of melibiose/cation symport of the melibiose permease of Salmonella typhimurium** *J. Biol. Chem* **286**:6367–6374

10. Hariharan P., Guan L. (2021) **Cooperative binding ensures the obligatory melibiose/Na+ cotransport in MelB** *J. Gen. Physiol* **153**

11. Jakkula S. V., Guan L. (2012) **Reduced Na(+) affinity increases turnover of Salmonella enterica serovar Typhimurium MelB** *J. Bacteriol* **194**:5538–5544

12. Katsube S., Liang R., Amin A., Hariharan P., Guan L. (2022) **Molecular Basis for the Cation Selectivity of Salmonella typhimurium Melibiose Permease** *J. Mol. Biol* **434**

13. Markham K. J., Tikhonova E. B., Scarpa A. C., Hariharan P., Katsube S., Guan L. (2021) **Complete cysteine-scanning mutagenesis of the Salmonella typhimurium melibiose permease** *J. Biol. Chem* **297**

14. Hariharan P., Tikhonova E., Medeiros-Silva J., Jeucken A., Bogdanov M. V., Dowhan W., Brouwers J. F., Weingarth M., Guan L. (2018) **Structural and functional characterization of protein-lipid interactions of the Salmonella typhimurium melibiose transporter MelB** *BMC Biol* **16**

15. Blaimschein N., Hariharan P., Manioglu S., Guan L., Muller D. J. (2023) **Substrate-binding guides individual melibiose permeases MelB to structurally soften and to destabilize cytoplasmic middle-loop C3** *Structure* **31**:58–67

16. Ethayathulla A. S., Yousef M. S., Amin A., Leblanc G., Kaback H. R., Guan L. (2014) **Structure-based mechanism for Na(+)/melibiose symport by MelB** *Nat. Commun* **5**

17. Guan L., Hariharan P. (2021) **X-ray crystallography reveals molecular recognition mechanism for sugar binding in a melibiose transporter MelB** *Commun Biol* **4**

18. Hariharan P., Bakhtiiari A., Liang R., Guan L., 107427 (2024) **Distinct roles of the major binding residues in the cation-binding pocket of the melibiose transporter MelB** *J. Biol. Chem* https://doi.org/10.1016/j.jbc.2024.107427

19. Hariharan P. *et al.* (2024) **Mobile barrier mechanisms for Na(+)-coupled symport in an MFS sugar transporter** *Elife* **12**

20. Wilson D. M., Wilson T. H. (1987) **Cation specificity for sugar substrates of the melibiose carrier in Escherichia coli** *Biochim Biophys Acta* **904**:191–200

21. Wilson T. H., Ding P. Z. (2001) **Sodium-substrate cotransport in bacteria** *Biochim Biophys Acta* **1505**:121–130

22. Damiano-Forano E., Bassilana M., Leblanc G. (1986) **Sugar binding properties of the melibiose permease in Escherichia coli membrane vesicles. Effects of Na(+) and H(+) concentrations** *J. Biol. Chem* **261**:6893–6899

23. Pourcher T., Zani M. L., Leblanc G. (1993) **Mutagenesis of acidic residues in putative membrane-spanning segments of the melibiose permease of Escherichia coli. I. Effect on Na(+)-dependent transport and binding properties** *J. Biol. Chem* **268**:3209–3215

24. Zani M. L., Pourcher T., Leblanc G. (1993) **Mutagenesis of acidic residues in putative membrane-spanning segments of the melibiose permease of Escherichia coli. II. Effect on cationic selectivity and coupling properties** *J. Biol. Chem* **268**:3216–3221

25. Leblanc G., Pourcher T., Zani M. L. (1993) **The melibiose permease of Escherichia coli: importance of the NH2-terminal domains for cation recognition by the Na+/sugar cotransporter** *Soc. Gen. Physiol. Ser* **48**:213–227

26. Ganea C., Pourcher T., Leblanc G., Fendler K. (2001) **Evidence for intraprotein charge transfer during the transport activity of the melibiose permease from Escherichia coli** *Biochemistry* **40**:13744–13752

27. Granell M., Leon X., Leblanc G., Padros E., Lorenz-Fonfria V. A. (2010) **Structural insights into the activation mechanism of melibiose permease by sodium binding** *Proc Natl Acad Sci U S A* **107**:22078–22083

28. Hariharan P., Guan L. (2017) **Thermodynamic cooperativity of cosubstrate binding and cation selectivity of Salmonella typhimurium MelB** *J. Gen. Physiol* **149**:1029–1039

29. Katsube S., Willibal K., Vemulapally S., Hariharan P., Tikhonova E., Pardon E., Kaback H. R., Steyaert J., Guan L. (2023) **In vivo and in vitro characterizations of melibiose permease (MelB) conformation-dependent nanobodies reveal sugar-binding mechanisms** *J. Biol. Chem* **299**

30. Feng J., Selvam B., Shukla D. (2021) **How do antiporters exchange substrates across the cell membrane? An atomic-level description of the complete exchange cycle in NarK** *Structure* **29**:922–933

31. Takemoto M., Lee Y., Ishitani R., Nureki O. (2018) **Free Energy Landscape for the Entire Transport Cycle of Triose-Phosphate/Phosphate Translocator** *Structure* **26**:1284–1296

32. Alhadeff R., Warshel A. (2015) **Simulating the function of sodium/proton antiporters** *Proc. Natl. Acad. Sci. U. S. A* **112**:12378–12383

33. Moradi M., Enkavi G., Tajkhorshid E. (2015) **Atomic-level characterization of transport cycle thermodynamics in the glycerol-3-phosphate:phosphate antiporter** *Nat. Commun* **6**

34. Selvam B., Yu Y.-C., Chen L.-Q., Shukla D. (2019) **Molecular Basis of the Glucose Transport Mechanism in Plants** *ACS Central Science* **5**:1085–1096

35. Ke M., Yuan Y., Jiang X., Yan N., Gong H. (2017) **Molecular determinants for the thermodynamic and functional divergence of uniporter GLUT1 and proton symporter XylE** *PLoS Comput. Biol* **13**

36. Cheng K. J., Selvam B., Chen L.-Q., Shukla D. (2019) **Distinct Substrate Transport Mechanism Identified in Homologous Sugar Transporters** *J. Phys. Chem. B* **123**:8411–8418

37. Selvam B., Mittal S., Shukla D. (2018) **Free Energy Landscape of the Complete Transport Cycle in a Key Bacterial Transporter** *ACS Central Science* **4**:1146–1154

38. Kimanius D., Lindahl E., Andersson M. (2018) **Uptake dynamics in the Lactose permease (LacY) membrane protein transporter** *Sci. Rep* **8**

39. Chan M. C., Selvam B., Young H. J., Procko E., Shukla D. (2022) **The substrate import mechanism of the human serotonin transporter** *Biophys. J* **121**:715–730

40. Jensen M. Ø., Yin Y., Tajkhorshid E., Schulten K. (2007) **Sugar Transport across Lactose Permease Probed by Steered Molecular Dynamics** *Biophys. J* **93**:92–102

41. Li J., Zhao Z., Tajkhorshid E. (2019) **Locking Two Rigid-body Bundles in an Outward-Facing Conformation: The Ion-coupling Mechanism in a LeuT-fold Transporter** *Sci. Rep* **9**

42. Gradisch R. *et al.* (2024) **Ligand coupling mechanism of the human serotonin transporter differentiates substrates from inhibitors** *Nat. Commun* **15**

43. Chen H., Ogden D., Pant S., Cai W., Tajkhorshid E., Moradi M., Roux B., Chipot C. (2022) **A Companion Guide to the String Method with Swarms of Trajectories: Characterization, Performance, and Pitfalls** *J. Chem. Theory Comput* **18**:1406–1422

44. Pan A. C., Sezer D., Roux B. (2008) **Finding Transition Pathways Using the String Method with Swarms of Trajectories** *J. Phys. Chem. B* **112**:3432–3440

45. Guan L., Jakkula S. V., Hodkoff A. A., Su Y. (2012) **Role of Gly117 in the cation/melibiose symport of MelB of Salmonella typhimurium** *Biochemistry* **51**:2950–2957

46. Zani M. L., Pourcher T., Leblanc G. (1994) **Mutation of polar and charged residues in the hydrophobic NH2-terminal domains of the melibiose permease of Escherichia coli** *J. Biol. Chem* **269**:24883–24889

47. Carrasco N., Antes L. M., Poonian M. S., Kaback H. R. (1986) **lac permease of Escherichia coli: histidine-322 and glutamic acid-325 may be components of a charge-relay system** *Biochemistry* **25**:4486–4488

48. Jo S., Kim T., Iyer V. G., Im W. (2008) **CHARMM-GUI: A web-based graphical user interface for CHARMM** *J. Comput. Chem* **29**:1859–1865

49. Zhu X., Thompson K. C., Martínez T. J. (2019) **Geodesic interpolation for reaction pathways** *J. Chem. Phys* **150**

50. Huang J., Rauscher S., Nawrocki G., Ran T., Feig M., de Groot B. L., Grubmüller H., MacKerell A. D. (2017) **CHARMM36m: an improved force field for folded and intrinsically disordered proteins** *Nat. Methods* **14**:71–73

51. Best R. B., Zhu X., Shim J., Lopes P. E. M., Mittal J., Feig M., MacKerell A. D. (2012) **Optimization of the Additive CHARMM All-Atom Protein Force Field Targeting Improved Sampling of the Backbone phi, psi and Side-Chain chi(1) and chi(2) Dihedral Angles** *J. Chem. Theory Comput* **8**:3257–3273

52. MacKerell A. D., Feig M., Brooks C. L. (2004) **Improved Treatment of the Protein Backbone in Empirical Force Fields** *J. Am. Chem. Soc* **126**:698–699

53. MacKerell A. D. *et al.* (1998) **All-atom empirical potential for molecular modeling and dynamics studies of proteins** *J. Phys. Chem. B* **102**:3586–3616

54. Klauda J. B., Venable R. M., Freites J. A., O'Connor J. W., Tobias D. J., Mondragon-Ramirez C., Vorobyov I., MacKerell A. D., Pastor R. W. (2010) **Update of the CHARMM All-Atom Additive Force Field for Lipids: Validation on Six Lipid Types** *J. Phys. Chem. B* **114**:7830–7843

55. Guvench O., Greene S. N., Kamath G., Brady J. W., Venable R. M., Pastor R. W., Mackerell Jr A. D. (2008) **Additive empirical force field for hexopyranose monosaccharides** *J. Comput. Chem* **29**:2543–2564

56. Guvench O., Hatcher E., Venable R. M., Pastor R. W., MacKerell A. D. (2009) **CHARMM Additive All-Atom Force Field for Glycosidic Linkages between Hexopyranoses** *J. Chem. Theory Comput* **5**:2353–2370

57. Jorgensen W., Chandrasekhar J., Madura J., Impey R., Klein M. (1983) **Comparison of simple potential functions for simulating liquid water** *J. Chem. Phys* **79**:926–935

58. Phillips J. C. *et al.* (2020) **Scalable molecular dynamics on CPU and GPU architectures with NAMD** *J. Chem. Phys* **153**

59. Singharoy A., Chipot C., Moradi M., Schulten K. (2017) **Chemomechanical Coupling in Hexameric Protein–Protein Interfaces Harnesses Energy within V-Type ATPases** *J. Am. Chem. Soc* **139**:293–310

60. Sugita Y., Okamoto Y. (1999) **Replica-exchange molecular dynamics method for protein folding** *Chem. Phys. Lett* **314**:141–151

61. Sugita Y., Kitao A., Okamoto Y. (2000) **Multidimensional replica-exchange method for free-energy calculations** *J. Chem. Phys* **113**:6042–6051

62. Kumar S., Bouzida D., Swendsen R. H., Kollman P. A., Rosenberg J. M. (1992) **The Weighted Histogram Analysis Method for Free-Energy Calculations on Biomolecules. 1. The Method** *J. Comput. Chem.* **13**:1011–1021

63. Grossfield A. **WHAM: the weighted histogram analysis method** Grossfield Lab

64. Smart O. S., Goodfellow J. M., Wallace B. A. (1993) **The pore dimensions of gramicidin A** *Biophys. J* **65**:2455–2460

## Author information

**Ruibin Liang**[3]
Department of Chemistry and Biochemistry, Texas Tech University, Lubbock, United States
ORCID iD: 0000-0001-8741-1520

**For correspondence:** rliang@ttu.edu
[3]Leading Contact

**Lan Guan**
Department of Cell Physiology and Molecular Biophysics, Center for Membrane Protein Research, Texas Tech University Health Sciences Center, School of Medicine, Lubbock, United States
ORCID iD: 0000-0002-2274-361X

**For correspondence:** lan.guan@ttuhsc.edu

## Editors

Reviewing Editor
**Qiang Cui**
Boston University, Boston, United States of America

Senior Editor
**Qiang Cui**
Boston University, Boston, United States of America

**Reviewer #1 (Public review):**

Summary:

Liang and Guan have studied the transport mechanism of Melbiose transporter MelB using the string method in collective variables and replica-exchange umbrella sampling simulations. The authors study the mechanism of substrate binding to the outward-facing state, conformational change of the transporter from outward-facing to inward-facing, and substrate unbinding from inward-facing state. In their analysis, they also highlight the effects of mutant D59C and the effect of sodium binding on the substrate transport process.

Strengths:

The authors employ a combination of string method and replica-exchange umbrella sampling simulation techniques to provide a complete map of the free energy landscape for sodium-coupled melibiose transport in MelB.

Weaknesses:

(1) Free energy barriers appear to be very high for a substrate transport process. In Figure 3, the transitions from IF (Inward facing) to OF (Outward facing) state appear to have a barrier

of 12 kcal/mol. Other systems with mutant or sodium unbound have even higher barriers. This does not seem consistent with previous studies where transport mechanisms of transporters have been explored using molecular dynamics.

(2) Figure 2b: The PMF between images 20-30 shows the conformation change from OF to IF, where the occluded (OC) state is the highest barrier for transition. However, OC state is usually a stable conformation and should be in a local minimum. There should be free energy barriers between OF and OC and in between OC and IF.

(3) String method pathway is usually not the only transport pathway and alternate lower energy pathways should be explored. The free energy surface looks like it has not deviated from the string pathway. Longer simulations can help in the exploration of lower free energy pathways.

(4) The conformational change in transporters from OF to IF state is a complicated multi-step process. First, only 10 images in the string pathway are used to capture the transition from OF to IF state. I am not sure is this number is enough to capture the process. Second, the authors have used geodesic interpolation algorithm to generate the intermediate images. However, looking at Figure 3B, it looks like the transition pathway has not captured the occluded (OC) conformation, where the transport tunnel is closed at both the ends. Transporters typically follow a stepwise conformational change mechanism where OF state transitions to OC and then to IF state. It appears that the interpolation algorithm has created a hourglass-like state, where IF gates are opening and OF gates are closing simultaneously thereby creating a state where the transport tunnel is open on both sides of the membrane. These states are usually associated with high energy. References 30-42 cited in the manuscript reveal a distinct OC state for different transporters.

https://doi.org/10.7554/eLife.103421.1.sa3

**Reviewer #2 (Public review):**

Summary:

The manuscript by Liang and Guan provides an impressive attempt to characterize the conformational free energy landscape of a melibiose permease (MelB), a symporter member of major facilitator superfamily (MFS) of transporters. Although similar studies have been conducted previously for other members of MFS, each member or subfamily has its own unique features that make the employment of such methods quite challenging. While the methodology is indeed impressive, characterizing the coupling between large-scale conformational changes and substrate binding in membrane transporters is quite challenging and requires a sophisticated methodology. The conclusions obtained from the three sets of path-optimization and free energy calculations done by the authors are generally supported by the provided data and certainly add to our understanding of how sodium binding facilitates the transport of melibiose in MelB. However, the data is not generated reliably which questions the relevance of the conclusions as well. I particularly have some concerns regarding the implementation of the methodology that I will discuss below.

(1) In enhanced sampling techniques, often much attention is given to the sampling algorithm. Although the sampling algorithm is quite important and this manuscript has chosen an excellent pair: string method with swarms of trajectories (SMwST) and replica-exchange umbrella sampling (REUS) for this task, there are other important factors that must be taken into account. More specifically, the collective variables used and the preparation of initial conformations for sampling. I have objectives for both of these (particularly the latter) that I detail below. Overall, I am not confident that the free energy profiles generated

(summarized in Figure 5) are reliable, and unfortunately, much of the data presented in this manuscript heavily relies on these free energy profiles.

(2) The authors state that they have had an advantage over other similar studies in that they had two endpoints of the string to work from experimental data. I agree that this is an advantage. However, this could lead to some dangerous flaws in the methodology if not appropriately taken into account. Proteins such as membrane transporters have many slow degrees of freedom that can be fully captured within tens of nanoseconds (90 ns was the simulation time used here for the REUS). Biased sampling allows us to overcome this challenge to some extent, but it is virtually impossible to take into account all slow degrees of freedom in the enhanced sampling protocol (e.g., the collective variables used here do not represent anything related to sidechain dynamics). Therefore, if one mixes initial conformations that form different initial structures (e.g., an OF state and an IF state from two different PDB files), it is very likely that despite all equilibration and relaxation during SMwST and REUS simulations, the conformations that come from different sources never truly mix. This is dangerous in that it is quite difficult to detect such inconsistencies and from a theoretical point of view it makes the free energy calculations impossible. Methods such as WHAM and its various offshoots all rely on overlap between neighboring windows to calculate the free energy difference between two windows and the overlap should be in all dimensions and not just the ones that we use for biasing. This is related to well-known issues such as hidden barriers and metastability. If one uses two different structures to generate the initial conformations, then the authors need to show their sampling has been long enough to allow the two sets of conformations to mix and overlap in all dimensions, which is a difficult task to do.

(3) I also have concerns regarding the choice of collective variables. The authors have split the residues in each transmembrane helix into the cyto- and periplasmic sides. Then they have calculated the mass center distance between the cytoplasmic sides of certain pairs of helices and have also done the same for the periplasmic side. Given the shape of a helix, this does not seem to be an ideal choice since rather than the rotational motion of the helix, this captures more the translational motion of the helix. However, the transmembrane helices are more likely to undergo rotational motion than the translational one.

(4) Convergence: String method convergence data does not show strong evidence for convergence (Figure S2) in my opinion. REUS convergence is also not discussed. No information is provided on the exchange rate or overlap between the windows.

https://doi.org/10.7554/eLife.103421.1.sa2

**Reviewer #3 (Public review):**

The paper from Liang and Guan details the calculation of the potential mean force for the transition between two key states of the melibiose (Mel) transporter MelB. The authors used the string method along with replica-exchange umbrella sampling to model the transition between the outward and inward-facing Mel-free states, including the binding and subsequent release of Mel. They find a barrier of ~6.8 kcal/mol and an overall free-energy difference of ~6.4 kcal/mol. They also investigate the same process without the co-transported $Na^+$, finding a higher barrier, while in the D59C mutant, the barrier is nearly eliminated.

I found this to be an interesting and technically competent paper. I was disappointed actually to see that the authors didn't try to complete the cycle. I realize this is beyond the scope of the study as presented.

The results are in qualitative agreement with expectations from experiments. Could the authors try to make this comparison more quantitative? For example, by determining the

diffusivity along the path, the authors could estimate transition rates.

Relatedly, could the authors comment on how typical concentration gradients of Mel and Na+ would affect these numbers?

https://doi.org/10.7554/eLife.103421.1.sa1

**Author response:**

> ***Reviewer 1:***
>
> *(1) Free energy barriers appear to be very high for a substrate transport process. In Figure 3, the transitions from IF (Inward facing) to OF (Outward facing) state appear to have a barrier of 12 kcal/mol. Other systems with mutant or sodium unbound have even higher barriers. This does not seem consistent with previous studies where transport mechanisms of transporters have been explored using molecular dynamics.*

First, in Figure 3, the transition from IF to OF state doesn't have a barrier of 12 kcal/mol. The IFF to OFB transition is almost barrierless, and from OFB to OFF is ~5 kcal/mol, which is also evident in Figure 2.

If the reviewer was referring to the transition from OFB to IFB states, the barrier is 6.8 kcal/mol (Na+ bound state), and the rate-limiting barrier in the entire sugar transport process (Na+ bound state) is 8.4 kcal/mol, as indicated in Figure 2 and Table 1, which is much lower than the 12 kcal/mol barrier the reviewer mentioned. When the Na+ is unbound, the barrier can be as high as 12 kcal/mol, but it is this high barrier that leads to our conclusion that the Na+ binding is essential for sugar transport, and the 12 kcal/mol barrier indicates an energetically unfavorable sugar translocation process when the Na+ is unbound, which is unlikely to be the major translocation process in nature.

Even for the 12 kcal/mol barrier reported for the Na+ unbound state, it is still not too high considering the experimentally measured MelB sugar active transport rate, which is estimated to be on the order of 10 to 100 s-1. This range of transport rate is typical for similar MFS transporters such as the lactose permease (LacY), which has an active transport rate of 20 s-1. The free energy barrier associated with the active transport is thus on the order of ~15-16 kcal/mol based on transition state theory assuming kBT/h as the prefactor. This experimentally estimated barrier is higher than all of our calculated barriers. Our calculated barrier for the sugar translocation with Na+ bound is 8.4 kcal/mol, which means an additional ~7-8 kcal/mol barrier is contributed by the Na+ release process after sugar release in the IFF state. This is a reasonable estimation of the Na+ unbinding barrier.

Therefore, whether the calculated barrier is too high depends on the experimental kinetics measurements, which are often challenging to perform. Based on the existing experimental data, the MFS transporters are

usually relatively slow in their active transport cycle. The calculated barrier thus falls within the reasonable range considering the experimentally measured active transport rates.

> *(2) Figure 2b: The PMF between images 20-30 shows the conformation change from OF to IF, where the occluded (OC) state is the highest barrier for transition. However, OC state is usually a stable conformation and should be in a local minimum. There should be free energy barriers between OF and OC and in between OC and IF.*

First, the occluded state (OCB) is not between images 20-30, it is between images 10 to 20. Second, there is no solid evidence that the OCB state is a stable conformation and a local

minimum. Existing experimental structures of MFS transporters seldom have the fully occluded state resolved.

> *(3) String method pathway is usually not the only transport pathway and alternate lower energy pathways should be explored. The free energy surface looks like it has not deviated from the string pathway. Longer simulations can help in the exploration of lower free energy pathways.*

We agree with the reviewer that the string method pathway is usually not the only transport pathway and alternate lower energy pathways could exist. However, we also note that even if the fully occluded state is a local minimum and our free energy pathway does visit this missing local minimum after improved sampling, the overall free energy barrier will not be lowered from our current calculated value. This is because the current rate-limiting barrier arises from the transition from the OFB state to the IFF state, and the barrier top corresponds to the sugar molecule passing through the most constricted region in the cytoplasmic region, i.e., the IFC intermediate state visited *after* the IFB state is reached. Therefore, the free energy difference between the OFB state and the IFC state will not be changed by another hypothetical local minimum between the OFB and IFB states, i.e., the occluded OCB state. In other words, a hypothetical local minimum corresponding to the occluded state, even if it exists, will not decrease the overall rate-limiting barrier and may even increase it further, depending on the depth of the local minimum and the additional barriers of entering and escaping from this new minimum.

> *(4) The conformational change in transporters from OF to IF state is a complicated multi-step process. First, only 10 images in the string pathway are used to capture the transition from OF to IF state. I am not sure is this number is enough to capture the process. Second, the authors have used geodesic interpolation algorithm to generate the intermediate images. However, looking at Figure 3B, it looks like the transition pathway has not captured the occluded (OC) conformation, where the transport tunnel is closed at both the ends. Transporters typically follow a stepwise conformational change mechanism where OF state transitions to OC and then to IF state. It appears that the interpolation algorithm has created a hourglasslike state, where IF gates are opening and OF gates are closing simultaneously thereby creating a state where the transport tunnel is open on both sides of the membrane. These states are usually associated with high energy. References 30-42 cited in the manuscript reveal a distinct OC state for different transporters.*

In our simulations, even with 10 initial images representing the OF to IF conformational transition, the occluded state is sampled in the final string pathway. There is an ensemble of snapshots where the extracellular and intracellular gates are both relatively narrower than the OF and IF states, preventing the sugar from leaking into either side of the bulk solution. In contrast to the reviewer's guess, we never observed an hourglass-like state in our simulation where both gates are open. Figure 3B is a visual representation of the backbone structure of the OCB state without explicitly showing the actual radius of the gating region, which also depends on the side chain conformations. Thus, Figure 3B alone cannot be used to conclude that we are dominantly sampling an hourglass-like intermediate conformation instead of the occluded state, as mentioned by the reviewer.

Moreover, not all references in 30-42 have sampled the occluded state since many of them did not even simulate the substrate translocation process at all. For the ones that did sample substrate translocation processes, only two of them were studying the cation-coupled MFS family symporter (ref 38, 40) and they didn't provide the PMF for the entire translocation process. There is no strong evidence for a stable minimum corresponding to a fully occluded state in these two studies. In fact, different types of transporters with different coupling

cations may exhibit different stability of the fully occluded state. For example, the fully occluded state has been experimentally observed for some MFS transporters, such as multidrug transporter EmrD, but not for others, such as lactose permease LacY. Thus, it is not generally true that a stable, fully-occluded state exists in all transporters, and it highly depends on the specific type of transporter and the coupling ion under study.

> ***Reviewer 2:***
>
> *The manuscript by Liang and Guan provides an impressive attempt to characterize the conformational free energy landscape of a melibiose permease (MelB), a symporter member of major facilitator superfamily (MFS) of transporters. Although similar studies have been conducted previously for other members of MFS, each member or subfamily has its own unique features that make the employment of such methods quite challenging. While the methodology is indeed impressive, characterizing the coupling between large-scale conformational changes and substrate binding in membrane transporters is quite challenging and requires a sophisticated methodology. The conclusions obtained from the three sets of path-optimization and free energy calculations done by the authors are generally supported by the provided data and certainly add to our understanding of how sodium binding facilitates the transport of melibiose in MelB. However, the data is not generated reliably which questions the relevance of the conclusions as well. I particularly have some concerns regarding the implementation of the methodology that I will discuss below.*
>
> *(1) In enhanced sampling techniques, often much attention is given to the sampling algorithm. Although the sampling algorithm is quite important and this manuscript has chosen an excellent pair: string method with swarms of trajectories (SMwST) and replica-exchange umbrella sampling (REUS) for this task, there are other important factors that must be taken into account. More specifically, the collective variables used and the preparation of initial conformations for sampling. I have objectives for both of these (particularly the latter) that I detail below. Overall, I am not confident that the free energy profiles generated (summarized in Figure 5) are reliable, and unfortunately, much of the data presented in this manuscript heavily relies on these free energy profiles.*

Since comments (1) and (2) from this review are related, please see our response to (2) below.

> *(2) The authors state that they have had an advantage over other similar studies in that they had two endpoints of the string to work from experimental data. I agree that this is an advantage. However, this could lead to some dangerous flaws in the methodology if not appropriately taken into account. Proteins such as membrane transporters have many slow degrees of freedom that can be fully captured within tens of nanoseconds (90 ns was the simulation time used here for the REUS). Biased sampling allows us to overcome this challenge to some extent, but it is virtually impossible to take into account all slow degrees of freedom in the enhanced sampling protocol (e.g., the collective variables used here do not represent anything related to sidechain dynamics). Therefore, if one mixes initial conformations that form different initial structures (e.g., an OF state and an IF state from two different PDB files), it is very likely that despite all equilibration and relaxation during SMwST and REUS simulations, the conformations that come from different sources never truly mix. This is dangerous in that it is quite difficult to detect such inconsistencies and from a theoretical point of view it makes the free energy calculations impossible. Methods such as WHAM and its various offshoots all rely on overlap between neighboring windows to calculate the free energy difference between two windows and the overlap should be in all dimensions and not just the ones that we use for biasing. This is related to well-known issues such as hidden barriers and metastability. If one uses two different structures to generate the initial conformations,*

> *then the authors need to show their sampling has been long enough to allow the two sets of conformations to mix and overlap in all dimensions, which is a difficult task to do.*

We partly agree with the reviewer in that it is challenging to investigate whether the structures generated from the two different initial structures are sufficiently mixed in terms of orthogonal degrees of freedom outside the CV space during our string method and REUS simulations. We acknowledge that our simulations are within 100 ns for each REUS window, and there could be some slow degrees of freedom that are not fully sampled within this timescale. However, the conjectures and concerns raised by the reviewer are somewhat subjective in that they are almost impossible to be completely disproven. In a sense, these concerns are essentially the same as the general suspicion that the biomolecular simulation results are not completely converged, which cannot be fully ruled out for relatively complex biomolecular systems in any computational study involving MD simulations. We also note that comparison among the PMFs of different cation bound/unbound states will have some error cancellation effects because of the consistent use of the same sampling methods for all three systems. Our main conclusions regarding the cooperative binding and transport of the two substrates lie in such comparison of the PMFs and additionally on the unbiased MD simulations. Thus, although there could be insufficient sampling, our key conclusions based on the relative comparison between the PMFs are more robust and less likely to suffer from insufficient sampling.

> *(3) I also have concerns regarding the choice of collective variables. The authors have split the residues in each transmembrane helix into the cyto- and periplasmic sides. Then they have calculated the mass center distance between the cytoplasmic sides of certain pairs of helices and have also done the same for the periplasmic side. Given the shape of a helix, this does not seem to be an ideal choice since rather than the rotational motion of the helix, this captures more the translational motion of the helix. However, the transmembrane helices are more likely to undergo rotational motion than the translational one.*

Our choice of CVs not only captures the translational motion but also the rotational motion of the helix. Consider a pair of helices. If there is a relative rotation in the angle between the two helices, causing the extracellular halves of the two helices to get closer and the intracellular halves to be more separated, this rotational motion can be captured as the decrease of one CV describing the extracellular distance and increase in the other CV describing the intracellular distance between the two helices. Reversely, if one of the two CVs is forced to increase and the other one forced to decrease, it can, in principle, bias the relative rotation of the two helices with respect to each other. Indeed, comparing Figure 3 with Figure S4, the reorientation of the helices with respect to the membrane normal (Fig. S4) is accompanied by the simultaneous decrease and increase in the pairwise distances between different segments of the helices. Therefore, our choice of CVs in the string method and REUS are not biased against the rotation of the helices, as the reviewer assumed.

> *(4) Convergence: String method convergence data does not show strong evidence for convergence (Figure S2) in my opinion. REUS convergence is also not discussed. No information is provided on the exchange rate or overlap between the windows.*

The convergence of string method, REUS, the exchange rate and overlap between windows will be discussed in the reviewed manuscript.

> ***Reviewer 3:***
>
> *The paper from Liang and Guan details the calculation of the potential mean force for the transition between two key states of the melibiose (Mel) transporter MelB. The*

> *authors used the string method along with replica-exchange umbrella sampling to model the transition between the outward and inwardfacing Mel-free states, including the binding and subsequent release of Mel. They find a barrier of ~6.8 kcal/mol and an overall free-energy difference of ~6.4 kcal/mol. They also investigate the same process without the co-transported Na+, finding a higher barrier, while in the D59C mutant, the barrier is nearly eliminated.*

For Na+ bound state, the rate-limiting barrier is 8.4 kcal/mol instead of 6.8 kcal/mol. The overall free energy difference is 3.7 kcal/mol instead of 6.4 kcal/mol. These numbers need to be corrected in the public review.

> *I found this to be an interesting and technically competent paper. I was disappointed actually to see that the authors didn't try to complete the cycle. I realize this is beyond the scope of the study as presented.*

We agree with the reviewer that characterizing the complete cycle is our eventual goal. However, in order to characterize the complete cycle of the transporter, the free energy landscapes of the Na+ binding and unbinding process in the sugar-bound and unbound states, as well as the OF to IF conformational transition in the apo state. These additional calculations are expensive, and the amount of work devoted to these new calculations is estimated to be at least the same as the current study. Therefore, we prefer to carry out and analyze these new simulations in a future study.

> *The results are in qualitative agreement with expectations from experiments. Could the authors try to make this comparison more quantitative? For example, by determining the diffusivity along the path, the authors could estimate transition rates.*

In our revised manuscript, we will determine the diffusivity along the path and estimate transition rates.

> *Relatedly, could the authors comment on how typical concentration gradients of Mel and Na+ would affect these numbers?*

The concentration gradient of Mel and Na+ can be varied in different experimental setups. In a typical active transport essay, the Na+ has a higher concentration outside the cell, and the melibiose has a higher concentration inside the cell. In the steady state, depending on the experiment setup, the extracellular Na+ concentration is in the range of 10-20 mM, and the intracellular concentration is self-balanced in the range of 3-4 mM due to the presence of other ion channels and pumps. In addition to the Na+ concentration gradient, there is also a transmembrane voltage potential of -200 mV (the intracellular side being more negative than the extracellular side), which facilitates the Na+ release into the intracellular side. In the steady state, the extracellular concentration of melibiose is ~0.4 mM, and the intracellular concentration is at least 1000 times the extracellular concentration, greater than 0.4 M. In this scenario, the free energy change of intracellular melibiose translocation will be increased by about ~5 kcal/mol at 300K temperature, leading to a total $\Delta G$ of ~8 kcal/mol. The total barrier for the melibiose translocation is expected to be increased by less than 5 kcal/mol. However, the increase in $\Delta G$ for intracellular melibiose translocation will be compensated by a decrease in $\Delta G$ of similar magnitude ( ~5 kcal/mol) for intracellular Na+ translocation. In a typical sugar self-exchange essay, there is no net gradient in the melibiose or Na+ across the membrane, and the overall free energy changes we calculated apply to this situation.

https://doi.org/10.7554/eLife.103421.1.sa0